

THE OFFICIAL MAGAZINE OF THE OCEANOGRAPHY SOCIETY

Oceanography

CITATION

Schönau, M.C., D.L. Rudnick, I. Cerovecki, G. Gopalakrishnan, B.D. Cornuelle, J.L. McClean, and B. Qiu. 2015. The Mindanao Current: Mean structure and connectivity. *Oceanography* 28(4):34–45, <http://dx.doi.org/10.5670/oceanog.2015.79>.

DOI

<http://dx.doi.org/10.5670/oceanog.2015.79>

COPYRIGHT

This article has been published in *Oceanography*, Volume 28, Number 4, a quarterly journal of The Oceanography Society. Copyright 2015 by The Oceanography Society. All rights reserved.

USAGE

Permission is granted to copy this article for use in teaching and research. Republication, systematic reproduction, or collective redistribution of any portion of this article by photocopy machine, reposting, or other means is permitted only with the approval of The Oceanography Society. Send all correspondence to: info@tos.org or The Oceanography Society, PO Box 1931, Rockville, MD 20849-1931, USA.

The Mindanao Current

Mean Structure and Connectivity

By Martha C. Schönau, Daniel L. Rudnick,
Ivana Cerovecki, Ganesh Gopalakrishnan,
Bruce D. Cornuelle, Julie L. McClean, and Bo Qiu

ABSTRACT. The Mindanao Current (MC), a low-latitude western boundary current in the Pacific Ocean, plays an important role in heat and freshwater transport to the western Pacific warm pool and the Indian Ocean. However, there have been relatively few comprehensive studies of the structure and variability of the MC and its connectivity to regional circulation. The Origins of the Kuroshio and Mindanao Current (OKMC) initiative combines four years of glider observations of the MC, a historical conductivity-temperature-depth (CTD)/float climatology, and results from a global strongly eddying forward ocean general circulation model simulation and a regional ocean state estimate. The MC is resolved as a strong southward current primarily within the upper 200 m, approaching 1 m s^{-1} , and extending roughly 300 km offshore of Mindanao. Observations and model simulations show a persistent northward Mindanao Undercurrent (MUC) below the thermocline. The MC transports water masses of North Pacific origin southward, while the MUC carries water with South Pacific characteristics northward. The subthermocline transport of the MC and the MUC is connected to other undercurrents in the Philippine Sea. The variability of this transport is a topic of continuing research.

MOTIVATION AND BACKGROUND

The Mindanao Current (MC) is a low-latitude western boundary current (LLWBC) in the North Pacific that is formed when the North Equatorial Current (NEC) bifurcates close to the Philippine Coast (e.g., Rudnick et al., 2015, in this issue). The MC transports and mixes North Pacific water masses as it flows south out of the Philippine Sea, feeding tropical circulation cells in both the North Pacific and the Indian Oceans (via the Indonesian throughflow [ITF]). The MC thus provides a pathway for heat and freshwater exchange between ocean basins (Gordon, 1986; Fine et al., 1994), and it carries climatic signals from higher latitudes into the tropics, influencing the El Niño-Southern Oscillation and regional climate (Lukas et al., 1996; Gu and Philander, 1997). The MC transport to the western Pacific warm pool also impacts available nutrients and marine ecosystem productivity (Bell, 2013). However, there have been relatively few observations of the MC that resolve its mean structure and its variability, making

it one of the least understood western boundary currents in the Pacific.

Here, we present observations and modeling results of the Mindanao Current that were part of the Origins of the Kuroshio and Mindanao Current (OKMC) initiative. OKMC is one of a few concurrent research efforts to understand water transport and exchange of LLWBCs in the western Pacific. Other research initiatives are Observations of Kuroshio Transport and Variability (OKTV; Yang et al., 2015, in this issue), the South Pacific Ocean and circulation and climate experiment (SPICE; Ganachaud et al., 2014), and Northwestern Pacific Climate and Ocean Circulation (NPOCE; Hu et al., 2015a). A goal of these projects is to evaluate the role of LLWBCs on tropical Pacific water mass exchange, the relationship of LLWBCs to local and regional climatic forcing, and the temporal and spatial scales of LLWBC variability (Ganachaud et al., 2014; Hu et al., 2015b). Challenges to observing and modeling the MC include a strong mean current, extreme topography, a remote

location, and the regional variability related to high-frequency wind-stress fluctuations and eddies. As observations and model simulations improve, they will be able to resolve and diagnose the complex dynamics and mixing processes of this intricate region.

During OKMC, gliders were deployed from Palau and made the round trip to the coast of Mindanao and back, with the goal of making repeated sections across the MC from June 2009 to January 2014. Data from historical conductivity-temperature-depth (CTD)/expendable CTD (X-CTD) profilers (2000–2014) and from profiling floats deployed during OKMC were combined to form a regional climatology. The regional circulation was simulated using two separate eddy-active ocean general circulation models (OGCMs) running in both forward (output from 2000 to 2009) and assimilative modes (2010–2011). We believe this to be one of the most comprehensive studies of the MC to date.

Until the OKMC project commenced in 2009, the most extensive series of observations were collected from 1987 to 1990 as part of two efforts: the Western Equatorial Pacific Ocean Circulation Study (WEPOCS; Lindstrom et al., 1987) and a joint United States/People's Republic of China Tropical Ocean Global Atmosphere (TOGA) program (Toole et al., 1990). In data from hydrographic and acoustic Doppler current profiler (ADCP) measurements collected during eight cruises, the MC was observed within 200 km of the coast, registering strong velocities in the upper 300 m (Lukas et al., 1991). Ship-based observations at 8°N showed a steady mean MC in approximate geostrophic balance and extremely variable flows offshore

(Wijffels et al., 1995). More recently, moorings have been deployed across the MC. A single mooring anchored within the MC for the period from 1999 to 2002 showed the existence of a strong shallow surface current with a mean velocity and variability of $1.3 \pm 0.2 \text{ m s}^{-1}$ at 100 m (Kashino, 2005). The strongest velocity was measured during boreal summer, and the strength was apparently modulated by the onset of the 2002 El Niño. The strengthening of the MC during the summer months and El Niño has been associated with the transport and bifurcation latitude of the NEC (Qiu and Lukas, 1996; Qu and Lukas, 2003; Hu et al., 2015b). However, the relationship between MC mean structure and variability and local and regional forcing is unresolved.

Two other relevant circulation features are the surface/thermocline Mindanao Eddy (ME; Wyrтки, 1961), characterized by cyclonic recirculation, and the northward-flowing subthermocline Mindanao Undercurrent (MUC; Hu et al., 1991; Qu et al., 1998). However, these highly variable features have not been unambiguously identified. The ME, defined as a persistent eddy that feeds into the MC,

is sometimes difficult to see in synoptic hydrographic sections (Wijffels et al., 1995; Kashino et al., 2013), yet it frequently appears as a mean feature and has been resolved using surface drifters (Lukas et al., 1991). The MUC, typically located within 200 km of the shore, has been studied using mooring and modeling efforts to determine whether it is a persistent northward flow (Qu et al., 2012; Zhang et al., 2014) or part of a variable anticyclonic eddy (Kashino et al., 2015). Due to the variability of the ME and the MUC, identifying these features and understanding their relationship to the regional circulation is an ongoing area of research.

We present glider and CTD/float observations and the results of two eddy-active OGCMs to identify the southward MC and a persistently northward MUC. We focus on the connectivity of circulation in the region, where connectivity is defined through the transport of water masses characterized by their potential temperature and salinity. Together, the data and the model simulations provide robust measures of the mean structure and transport of both the MC and

MUC. Model simulations give estimates of monthly variability. The transports of water masses from model simulations and from observations are compared. The combination of a diverse array of observations and model simulations provides insight into the mean structure of the MC and MUC, their temporal variability, and their regional connectivity.

GLIDER OBSERVATIONS

The Spray glider (Sherman et al., 2001) is an autonomous underwater vehicle that flies horizontally on wings and profiles by changing buoyancy. The glider missions described here lasted about four months, traveling a distance of around 2,500 km while profiling to a depth of 1,000 m. Each dive cycle took about six hours, during which time the glider traveled 6 km horizontally. The glider measured temperature, salinity, and pressure with a Sea-Bird CTD and fluorescence with a Seapoint fluorometer.

Spray gliders were deployed from Palau at 7.5°N , 134.4°E and made profiles westward toward the island of Mindanao, crossing the MC at latitudes ranging from 6°N to 10.2°N (Figure 1). The goal was to make sections across the MC to the 1,000 m isobath, with the additional challenge of maneuvering through a strong and variable eddy field offshore. Ten gliders were deployed from June 2009 to July 2014, collecting 6,387 profiles of the region, traveling a total distance of 26,000 km, and making 19 sections of the MC. The interpretation of glider data was made challenging by the gliders' inability to follow exactly the same trajectory during every mission. To quantify the mean structure of the MC, we chose to project data along a line that is roughly parallel to the gradients of both the mean dynamic topography (MDT; AVISO/Cnes; <http://www.avis0.altimetry.fr>) and the bottom topography (Figure 1). Observations within 80 km of a line from 8.16°N , 126.61°E to 8.77°N , 130°E (hereafter referred to as the "mean line") were projected and objectively mapped. The resulting map is thus a

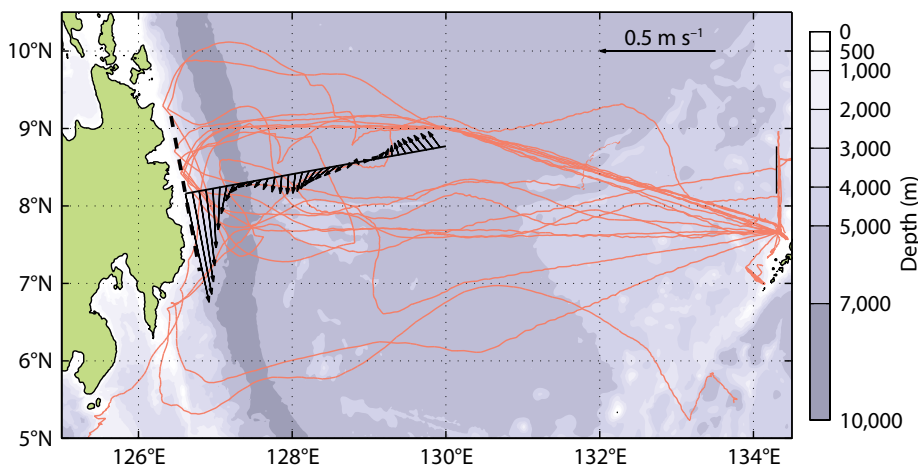


FIGURE 1. Trajectories of Spray gliders deployed from Palau (orange) displayed with topography (V18.1; Smith and Sandwell, 1997). The solid black line is the "mean line" described in the text (8.16°N , 126.61°E to 8.77°N , 130°E). The mean line extends from the 1,000 m isobath inshore to 380 km offshore. It is perpendicular to the bathymetry and the mean dynamic topography (indicated by the dashed black line) at the coast of Mindanao. Velocity profiles within 80 km of the solid black line are objectively mapped onto the line. Arrows indicate the depth-averaged velocity, averaged from the surface to 1,000 m, along this line; velocity is strongest near the coast of Mindanao.

spatial and temporal average of these profiles. Gliders provided a depth-average velocity based on dead reckoning of the glider's position (Todd et al., 2011; Davis et al., 2012). Following the projection and objective map, the mapped depth-average velocity was found to be perpendicular to the mean line (Figure 1), verifying that the current did flow parallel to the MDT, so that this was a reasonable line upon which to create a mean section. The error in depth-average velocity is estimated to be about 0.01 m s^{-1} (Todd et al., 2011; Davis et al., 2012). The error is random from glider to glider, and is thus reduced when averaging observations from multiple glider deployments. The depth-average velocity was used as a reference to calculate absolute geostrophic velocity using the thermal wind equation.

CTD/FLOAT OBSERVATIONS

To provide a broad-scale context of the MC, we collected profiling float temperature-salinity (T-S) data from the OKMC and the international Argo projects (<http://www.usgoda.gov>) in the low-latitude northwestern Pacific for a time period of 2001–2014. To enhance the quantity of the T-S data, especially off the Philippine coast, we also extracted available CTD and X-CTD data in the 0°N – 35°N , 115°E – 150°E domain archived by the US National Oceanographic Data Center (NODC) and the Japan Oceanographic Data Center (JODC). For data quality control, we compared the individually measured T-S values against the *World Ocean Atlas 2013* climatological data. T-S data were excluded if they fell outside of the two standard deviation envelopes of the local climatological T-S curve. For the float and CTD/X-CTD profiles that passed the quality control procedure, the T-S were first interpolated onto a regular 10 m vertical grid between the surface and 2,000 m. At each depth, T-S values were then mapped onto a $1/8^{\circ} \times 1/8^{\circ}$ grid using an objective mapping technique. For details of the mapping's weight function and decorrelation scales, readers are referred to Qiu et al. (2015, in this

issue). The CTD/float climatology was used to calculate the geostrophic velocity of the MC, referenced to 2,000 m, along 8.5°N . The horizontal geostrophic velocities averaged over increasing depth ranges in the upper 1,000 m provided further information about the spatial structure of the MC and its connectivity to the region.

OCEAN STATE ESTIMATE

The ocean state estimates were made using the Estimating the Circulation and Climate of the Ocean (ECCO) state estimation framework, which is based on the MIT General Circulation Model (MITgcm; Marshall et al., 1997) and its adjoint model. The ECCO framework implements a non-incremental four-dimensional variational (4D-Var) method (Heimbach et al., 2002), which adjusts control variables to minimize the sum of squared normalized misfits

are calculated at the space and time locations of the observations and normalized by the observation uncertainties (which include model representation errors). Observations used included satellite altimeter along-track sea surface height (SSH), separated into temporal mean and anomalies; gridded satellite sea surface temperature (SST); and Spray glider and Argo temperature and salinity profiles. Only observations within a region, chosen to be 122°E – 170°E and 5°N – 20°N , were used in order to focus on the region of interest and to speed the convergence of the estimates. The state estimation experiments assimilated these observations with one-month assimilation windows over a period from January 2010 to December 2011.

The model domain extended from 15°S to 27°N and from 115°E to 170°E . The maximum bottom depth is at

“ The [Mindanao Current] provides a pathway for heat and freshwater exchange between ocean basins, and it carries climatic signals from higher latitudes into the tropics, influencing the El Niño-Southern Oscillation and regional climate. ”

between a model simulation and observations, plus the sum of squared normalized control adjustments over a specified period of time. Control variables determine a dynamically consistent simulation (Le Dimet and Talagrand, 1986; Wunsch, 1996). The controls used here are temperature and salinity initial conditions, open boundary conditions, and atmospheric forcing fields. The control adjustments are normalized by the standard deviation of the control variable uncertainty. The observation-model misfits

6,500 m, and the bathymetry is from the ETOPO-2 two-minute gridded global topography. The model was integrated on a $1/6^{\circ} \times 1/6^{\circ}$ ($\sim 18 \text{ km}$) spherical polar grid, with 50 vertical levels. The levels spacing was 2.5 m at the surface gradually increasing with depth to a maximum of 300 m near the bottom. The model first-guess controls are described in Qiu et al. (2015, in this issue).

The MITgcm velocity (2010–2011) and its variability are calculated along the mean line (Figure 1). Horizontal maps of

salinity and velocity averaged on potential density surfaces provide regional circulation for the thermocline and subthermocline. For brevity, when comparing to other results, the ocean state estimate will be referred to as the MITgcm.

PARALLEL OCEAN PROGRAM (POP) SIMULATION

To provide a large scale and long period context for the observations and the adjoint MITgcm simulation, we used output from a forward strongly eddying (1/10°) global Parallel Ocean Program (POP) simulation. The POP simulation is a z -level ocean general circulation model that solves the three-dimensional primitive equations for ocean temperature, salinity, and momentum (Dukowicz and Smith, 1994). It has an implicit free surface. Partial bottom cells were used for improved representation of flow over the bottom boundary. This configuration has 42 vertical levels whose thicknesses ranges from 10 m in the uppermost level to 250 m in the deep ocean.

The POP simulation was coupled to a sea ice model (CICE) in the Community Earth System Model (CESM) framework. It was forced with Coordinated Ocean Research Experiment 2 inter-

annually varying atmospheric forcing (CORE2-IAF) from 1948 to 2009 (Large and Yeager, 2009). CORE2 fluxes are based upon six-hourly (1948–2006) near-surface vector wind, specific humidity, density, and air temperature based on National Center for Environmental Prediction (NCEP) reanalysis, daily downward radiation (1984–2006) from International Satellite Cloud Climatology Project (ISCCP) data (Zhang et al., 2004), and monthly precipitation (1979–2006) from a combination of satellite observations. The ocean model was initialized from rest using potential temperature and salinity from the World Hydrographic Program Special Analysis Center (WHP SAC) climatology (Gouretski and Koltermann, 2004).

Potential temperature, salinity, and velocity are analyzed for years 2000–2009. These variables were accumulated at every model step over the averaging period, in this case, a month. At the end of the month, the total sum is divided by the accumulation period. The POP mean velocity along the mean line (Figure 1), and the standard deviation of monthly averages can be compared with that of the MITgcm. Horizontal maps of salinity and velocity averaged between

potential density surfaces are compared to the MITgcm and CTD/float results. For simplicity, we will refer to the POP simulation only by the acronym POP.

MINDANAO CURRENT (MC) AND MINDANAO UNDERCURRENT (MUC)

Velocity and Transport

Observations and models of the mean velocity all reveal a strong MC and a clearly identifiable undercurrent. The mean geostrophic velocity of the glider observations, referenced to the mean depth-average velocity of the gliders, and the absolute velocities of the model simulations are compared along the mean line. The geostrophic velocity from the CTD/float climatology is along a latitudinal line at 8.5°N, extending from 126.8°E to 135°E. Although these results are averaged within different timeframes, they provide comparable estimates of the MC and MUC structure, as discussed below. Here, we use the terminology poleward (equatorward) to refer to flow that is perpendicular to the mean line in the north-northwest (south-southwest) direction for the glider and model simulations, and north (south) for the CTD/float observations. The core of the MC and location of the MUC are identified in each result.

Glider observations may best resolve the structure of the MC and advantageously have an absolute reference velocity. The absolute geostrophic velocity of the glider observations (Figure 2a) indicates the MC to have a maximum velocity core of -0.98 m s^{-1} centered near 127°E (50 km offshore) at a depth of 100 m. The equatorward velocity extends to a depth of 1,000 m near the coast and to roughly 250–300 km offshore at the surface. There is a second core of stronger equatorward flow at 128.9°E (250–350 km offshore) that may be associated with an offshore eddy. A poleward mean flow, the MUC, is visible below potential density surface 26 kg m^{-3} , with a maximum velocity core of 0.15 m s^{-1} centered at 127.2°E (75 km offshore) and potential density

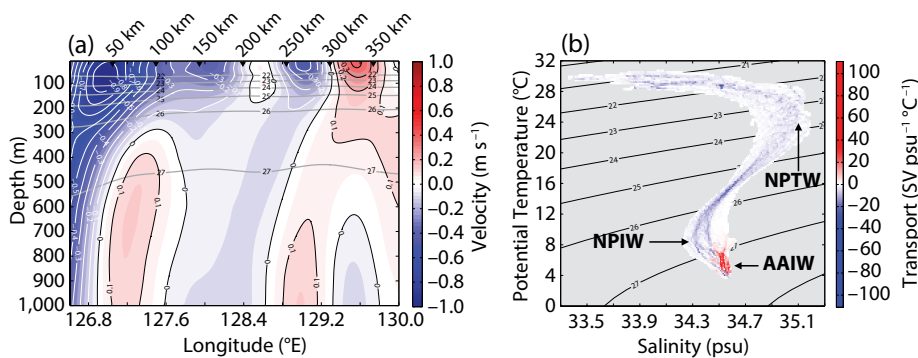


FIGURE 2. (a) Absolute geostrophic velocity perpendicular to the line 8.16°N, 126.61°E to 8.77°N, 130°E obtained from glider observations within 80 km of the line. The velocity is referenced to the depth-average velocity along the line shown in Figure 1. White contours indicate equatorward velocity (blue indicates negative) and black contours indicate poleward velocity (red indicates positive) at 0.1 m s^{-1} intervals. Potential density is shown in gray. (b) Transport binned potential temperature-salinity (T-S) diagram obtained by binning the cross-track transport of individual glider sections from the coast to 130°E, and surface to 1,000 m. Cross-track transport from each glider section within this area is summed in 0.01 psu and 0.2°C bins and divided by the number of sections and the bin size. Integrating the diagram gives a mean cross-track transport of all sections. Equatorward transport of salinity extrema North Pacific Tropical Water (NPTW) and North Pacific Intermediate Water (NPIW) is negative (blue), and poleward Mindanao Undercurrent (MUC) transport characteristic of Antarctic Intermediate Water (AAIW) is positive (red).

27.2 kg m⁻³ (650 m depth).

In contrast to the glider observations, the CTD/float geostrophic velocity is referenced to zero at 2,000 m (Figure 3a). The CTD/float velocity shows the MC extending to 500 m depth, with a maximum velocity of 0.4 m s⁻¹ in the upper 100 m. The MUC is against the coast, directly below the MC, with a maximum poleward velocity of 0.05 m s⁻¹ centered at 127.2°E and near 850 m, deeper than that of the glider but at the same longitude. The difference in angle (~10°) between the CTD/float observations and the glider observations is unlikely to cause large differences in the geostrophic velocity. Due to the lack of near coast T-S measurements, the deep expression of the equatorward MC against the Mindanao coast that is detected in glider observations (Figure 2a) is not resolved by the in situ float measurements. Referencing the CTD/float climatology to 2,000 m may also cause substantial differences between the geostrophic velocity of the climatology and that of the mean glider section, as the glider section is referenced to an absolute measure of velocity. Near the surface, the CTD/float climatology shows a secondary equatorward velocity maximum near 129°E and a poleward flow at 130°E, similar to the offshore structure of the mean glider section. This cyclonic offshore structure appears characteristic of the ME.

The mean velocity structures of the MITgcm and POP (Figure 4a,b) both show a strong equatorward MC core similar in magnitude to that of the glider, with perceptible yet weaker poleward undercurrents. The MITgcm has a maximum velocity of -0.98 m s⁻¹, located between the surface and 100 m, and equatorward velocity extending to 1,000 m (Figure 4a), in notable agreement with glider observations. In the MITgcm, the MUC is at 127.6°E, further offshore than in the glider observations, with a maximum velocity of 0.02 m s⁻¹ near 27.2 kg m⁻³ (700 m). In POP, an equatorward flowing MC extends to 600 m and has a maximum velocity of -0.82 m s⁻¹

at 200 m (Figure 4b). The POP MUC is directly below the MC, with a maximum velocity of about 0.04 m s⁻¹ centered at 27.2 kg m⁻³ (700 m) and 127.6°E. Unlike the glider observations and the MITgcm results, the POP undercurrent abuts the coast, and it is much wider, extending offshore 200 km. Near the surface, neither

simulation shows the double core structure typical of the ME apparent in the observations. Instead, both the MITgcm and POP show a weakening equatorward flow progressively offshore, with the MITgcm remaining slightly stronger than POP at 130°E.

To summarize, the MC and MUC

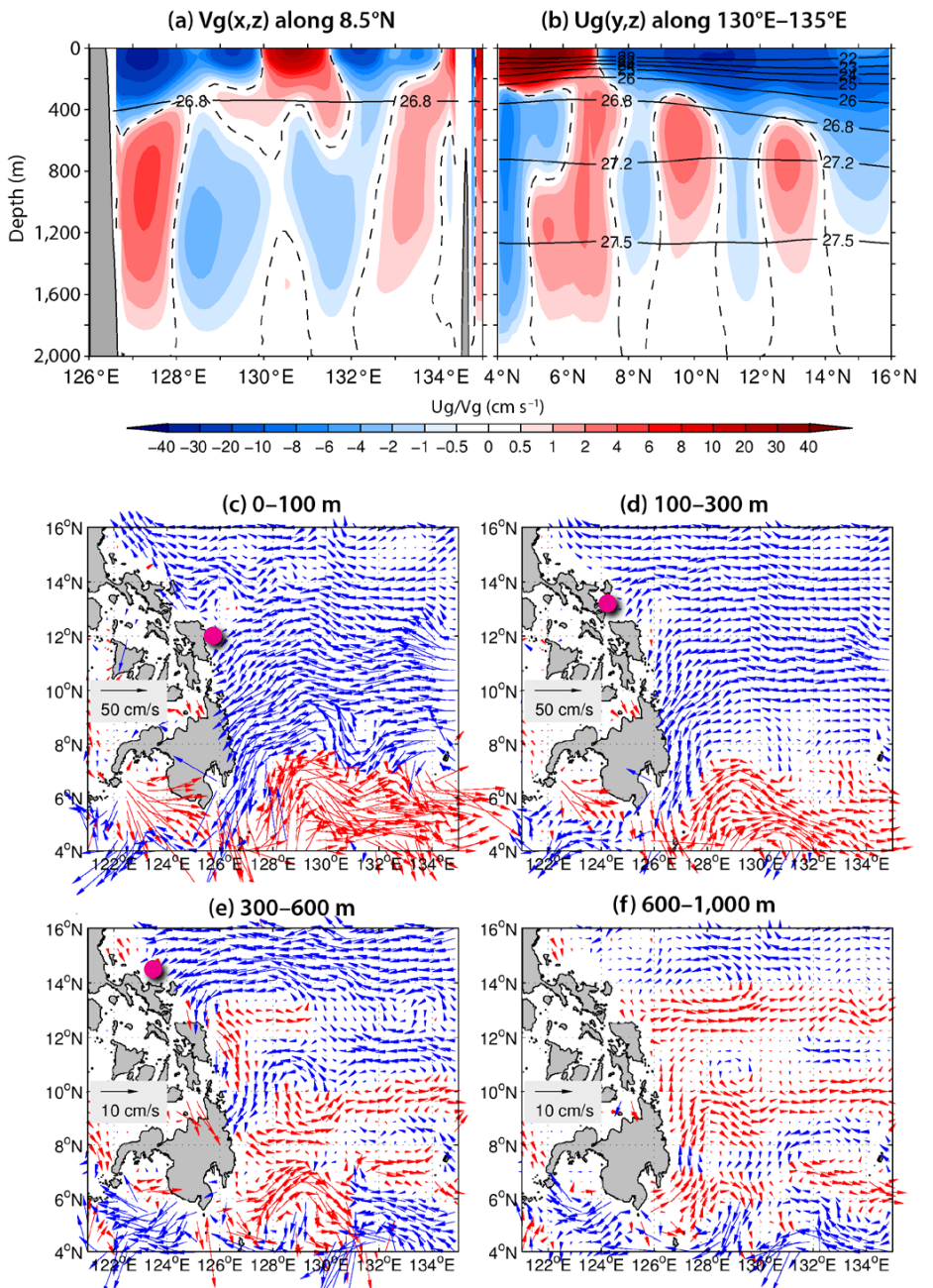


FIGURE 3. Conductivity-temperature-depth (CTD)/float observations of (a) longitude-depth section of meridional geostrophic velocity along 8.5°N, and (b) latitude-depth section of density (solid contours) and zonal geostrophic velocity (color shading) along 130°E–135°E. (c)–(f) Velocity vectors from CTD/float climatology are averaged in (c) 1–100 m, (d) 100–300 m, (e) 300–600 m, and (f) 600–1,000 m layers. Velocity vectors with eastward (westward) components are plotted in red (blue). The magenta dots indicate the bifurcation latitude of the North Equatorial Current (NEC).

means are stronger in the glider observations than in the CTD/float observations, and the MUC is stronger than depicted by the model simulations. However, the observations and model simulations all capture the shallow mean MC and a poleward undercurrent. The model simulations tend to have a strong MC core, similar to the glider observations, and weak equatorward flow extending to 130°E. Near the coast, the glider observations and the MITgcm show the MC extending to 1,000 m, with the MUC slightly offshore, whereas POP has the MUC directly below the MC and extending much further offshore. The differences near the coast are likely due to the MITgcm assimilation of glider observations, which better resolve coastal structure. Offshore observations show a cyclonic double-core structure that may indicate a quasi-permanent eddy, although it is not present in the model simulations.

Equatorward transports of the MC from the coast to 300 km offshore and from the surface to 1,000 m depth are -36.1 Sv (10^6 m³ s⁻¹) (glider), -18.2 Sv (CTD/float), -31.1 Sv (MITgcm), and -23.9 Sv (POP). Poleward transports of the MUC, defined as northward transport within 250 km of the coast and from the surface to 1,000 m, are 5.4 Sv (glider), 4.6 Sv (CTD/float), 1.7 Sv (MITgcm), and 5.7 Sv (POP). The model transports were integrated by depth on their respective spatial grids, and components were summed along the angled mean glider line. The bounds of integration provide a relative comparison of the transports of the MC and MUC across observational and model simulations, and were chosen based on the mean velocity fields. The MITgcm and glider show similar transports for the MC. The smaller transport of the CTD/float climatology is likely due to the reference level for velocity and

the inability to resolve the coastal structure. The smaller POP transport may be due to longer temporal averaging, leading to weaker equatorward flow or lack of flow near the coast. The undercurrent transports were similar. The weaker mean MITgcm undercurrent may be due to the large temporal and spatial variability of the MUC, discussed below.

Variability of Velocity and Transport

To estimate the variability of the MC and MUC, we calculate the standard deviation from monthly velocity fields of the MITgcm (Figure 4c) and POP (Figure 4d). Not surprisingly, the variability is highest near the core of the MC where the velocities are strongest. The maximum standard deviation of the MITgcm velocity is 0.23 m s⁻¹ in the core of the MC, and that of POP is 0.29 m s⁻¹ nearer to the surface than the maximum velocity core, which is deeper in POP than in the MITgcm. The standard deviation near the core is about 25% of the mean velocity. Near the coast, and deeper than 400 m, both models show an elevated standard deviation that exceeds the mean velocity. The variability suggests that the undercurrent meanders in the across-shore direction, and varies in strength. At the surface, the MITgcm has a standard deviation of 0.15 m s⁻¹ centered at 129°E (250–350 km offshore; Figure 4c). This high variability is the location of the surface ME, apparent in both glider and CTD/float observations (Figures 2a and 3a). Although the ME is not represented in the mean, it appears that the MITgcm captures some of its transient nature month to month.

Water Masses

The MC and MUC are major pathways for meridional transport of water masses in the tropical Pacific. Commonly identified water masses in the MC originate in the North Pacific and are identified by their salinity extrema (Lukas et al., 1991; Bingham and Lukas, 1994; Fine et al., 1994). The North Pacific Tropical Water (NPTW), a subsurface salinity

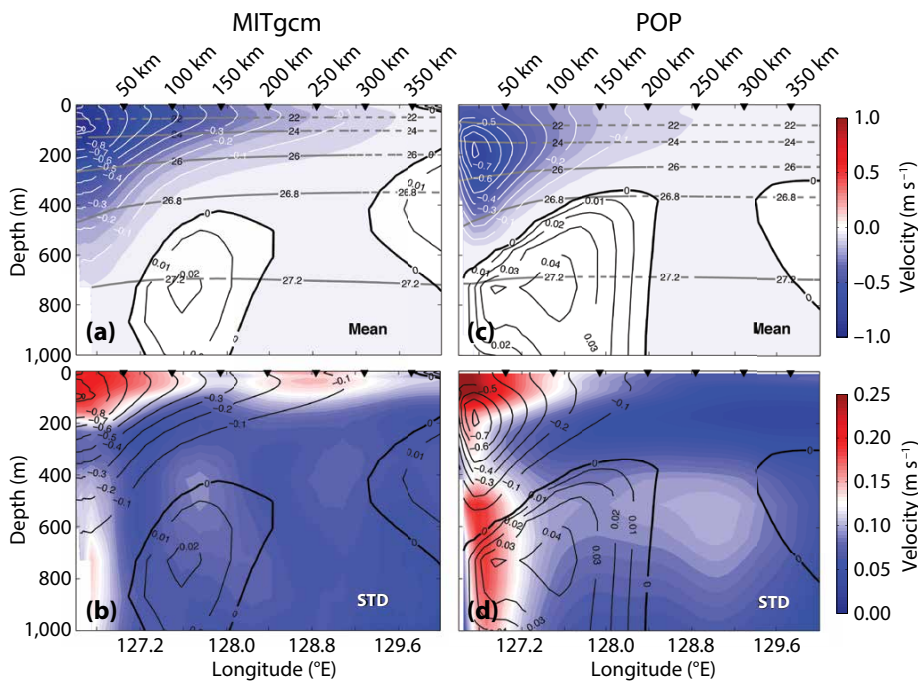


FIGURE 4. Time-averaged mean velocity from (a) the MIT General Circulation Model (MITgcm) (2010–2011), and (b) the Parallel Ocean Program (POP) simulation (2000–2009), and standard deviations of velocity between monthly averages for the (c) MITgcm (2010–2011), and (d) POP simulation (2000–2009). In (a) and (b), color and black contours indicate mean velocity perpendicular to the glider mean line, 8.16°N, 126.61°E to 8.77°N, 130°E. Equatorward velocity (blue indicates negative) is contoured white at 0.1 m s⁻¹ intervals, and poleward velocity (red indicates positive) is contoured black at 0.05 m s⁻¹ intervals. Gray contours are mean potential density. In (c) and (d), color is the magnitude of standard deviation, and black contours are the mean velocity contours from the MITgcm and the POP simulation from (a) and (b).

maximum, is found at a depth of less than 200 m and has salinity near 35 psu. The North Pacific Intermediate Water (NPIW), a subsurface salinity minimum, occurs between 300 m and 500 m depth, with salinity less than 34.4 psu.

The transport of NPTW and NPIW by the MC can be identified on a potential T-S binned transport diagram constructed using glider observations (Figure 2b), with the cross-track geostrophic transport computed for each glider section from the coast out to 130°E. The transport is binned in 0.01 psu and 0.2°C increments, the bins are summed over all glider sections, and then the bins are normalized by the number of sections and bin size. Integrating the T-S binned transport diagram thus yields the mean cross-track transport over all the sections. The equatorward transport by the MC (blue) of NPTW is identifiable as the salinity maximum near potential density 23.5 kg m⁻³, and that of NPIW as the salinity minimum near potential density 26.5 kg m⁻³. The poleward transport of the MUC (red) at densities greater than 27 kg m⁻³ is a striking feature. The density of 27.2 kg m⁻³ and salinity greater than 34.5 psu indicates advection of Antarctic Intermediate Water (AAIW), which originates in the South Pacific and has a higher oxygen content than surrounding NPIW (Tsuchiya et al., 1989; Tsuchiya, 1991; Bingham and Lukas, 1995; Qu and Lindstrom, 2004). The MUC transport is of particular interest due to the variability of the undercurrent and its uncertain connectivity to the rest of the region.

REGIONAL CONNECTIVITY Thermocline Circulation and Water Mass Transport

The surface and thermocline circulation in the Philippine Sea and its connectivity to the Mindanao Current are important in the transport of water masses from the subtropical North Pacific into the tropics (Fine et al., 1994). We highlight two uses of the observations and model simulations: detailing the structure of the MC as it originates at the bifurcation of the

NEC using the CTD/float climatology, and tracking the advection and decay of NPTW from the NEC to the MC using MITgcm and glider observations.

To examine the origins of the MC, CTD/float maps of the velocity field are shown from 0 m to 100 m (Figure 3c) and from 100 m to 300 m (Figure 3d). Arrow color indicates westward (blue) and eastward (red) flow. The NEC north of 7.5°N extends westward from 135°E to the coast of the Philippine islands, and the MC originates from the westward-impinging NEC (Figure 3c,d). A meridional cross section of the NEC geostrophic velocity averaged from 130°E to 135°E (Figure 3b) shows the strong westward surface current (blue) and the subthermocline undercurrents (red). The NEC extends to greater depths to the north, consistent with a downward sloping thermocline (Figure 3b). The bifurcation latitude of the NEC, shown by the magenta dots in Figure 3c–e, also shifts north with depth. As such, the MC has a more northern origin with depth. The horizontal pattern of velocity vectors in the upper ocean (above 300 m) suggests that the oscillating meridional flows east of the main body of the MC are associated with the NEC undulation that is possibly induced by the presence of the meridionally

aligned Palau ridge along ~135°E.

In the thermocline, the evolution of the NPTW salinity maximum is of interest. It decays along the Philippine coast, but is still identifiable into the Celebes (Sulawesi) Sea, and can be used as tracer (Gordon, 1986; Field and Gordon, 1992; Fine et al., 1994). We focus on NPTW by averaging the MITgcm mean salinity and velocity fields on potential density surfaces from 23.5 to 24 kg m⁻³ (Figure 5a). Black lines indicate the mean glider sections across the NEC (7.5°N–17°N, 134.3°E; Schönau and Rudnick, 2015) and MC (Figure 1). In the MITgcm at 134.3°E, the NPTW salinity is greater than 34.96 psu. As the NPTW is advected westward by the NEC, the salinity maximum decays. The layer including the NPTW bifurcates at the coast (near 13°N) where the salinity maximum is less than 34.92 psu. The NPTW is advected by the MC along the coast of the Philippines as a tongue of high salinity that decreases until it becomes indiscernible at 6°N. The decrease in salinity of this tongue is roughly 0.1 psu.

The decay of the salinity maximum of NPTW in the MC from model simulations can be compared to observations from a glider that was advected downstream by the MC. The trajectory of this

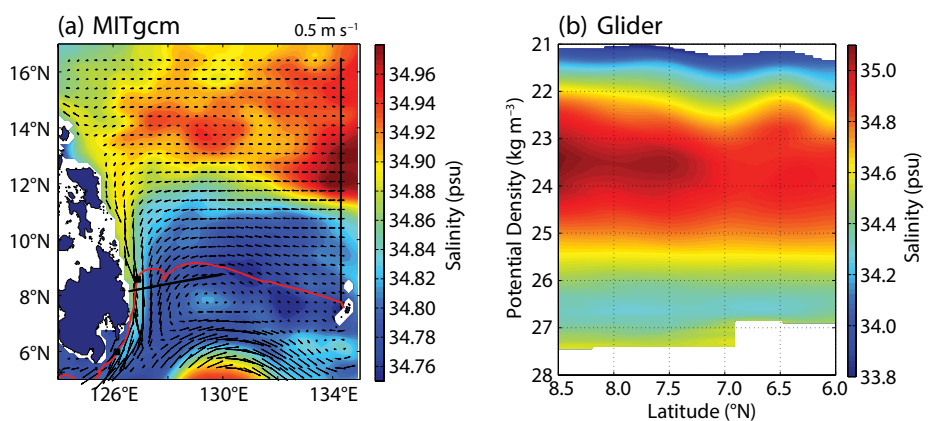


FIGURE 5. Advection of North Pacific Tropical Water (NPTW): (a) Horizontal map of velocity (arrows) and salinity (color) averaged over potential density range 23.5 to 24 kg m⁻³ from the MIT General Circulation Model (MITgcm). (b) Objectively mapped salinity on potential density surfaces from a glider deployed in April 2011. Black solid lines in panel (a) indicate lines where glider observations have been averaged as part of the Origins of the Kuroshio and Mindanao Current project (OKMC) for the North Equatorial Current (NEC) and the Mindanao Current (MC); the glider trajectory is shown as a red line. Black squares along this trajectory show the beginning and the end of the objectively mapped along-track salinity shown in panel (b). Both the MITgcm and the glider transect show a decrease in the subsurface salinity maximum of NPTW as it is advected along the coast.

glider, deployed in April 2011, is shown in Figure 5a (red line). The glider lost its steering capability, but not its ability to profile, so it acted as a profiling float in the MC until it was deposited in the Celebes (Sulawesi) Sea. An objective map of the along-track salinity on potential density surfaces (Figure 5b) shows a decay of NPTW along the coast. Although the salinity values are greater in the observations than in the model, the relative decay is similar. The success of the MITgcm in showing a clear decrease in salinity along the path of the MC breeds optimism that a more complete analysis will quantify the mixing processes.

Subthermocline Circulation

The dynamics, connectivity, and origins of the subthermocline circulation in the western Pacific are of particular interest as they are not well understood in this region. The geostrophic flow from the CTD/float climatology provides an introduction to the general patterns of subthermocline circulation in the Philippine Sea. The connectivity of certain undercurrents can be confirmed using glider observations of water mass transport.

The geostrophic flow of the MUC from the CTD/float climatology extends

down to 2,000 m (Figure 3a), and velocity maps suggest that the MUC is coherent along the entire coast of Mindanao from 5°N to 13°N (Figure 3f). Following its path along Mindanao, portions of the MUC are “peeled” away at roughly 6°N, 10°N, and 13°N (Figure 3f). These latitudes correspond to the locations of the eastward subthermocline jets (see Figure 3b) that are formed in the eastern part of the North Pacific basin (Qiu et al., 2013a) and that are revealed by Argo to be persistent across the Pacific (Qiu et al., 2013b).

The pattern of MUC circulation to the interior of the Philippine Sea can be compared between model simulations and observations. Maps of the MITgcm and POP mean salinity and velocity are constructed on potential density surfaces, averaged from 27 to 27.3 kg m⁻³ (Figure 6a,b). The potential density range encompasses the cores of the undercurrents beneath the MC and the NEC, and corresponds roughly to the 600–1,000 m depth range in the CTD/float climatology (Figure 3f). The poleward flow of the MUC is visible in both models (Figure 6a,b) near 8°N. In the MITgcm, a weak MUC transports high-salinity water north and east, forming an anticyclonic

recirculation east of 130°E and feeding the southern NEUC (Figure 6a). In POP (Figure 6b), the MUC both feeds the southern NEUC near 8°N and continues to flow poleward. The poleward and eastward POP pattern is similar to that of the CTD/float climatology (Figure 3f).

It should be noted that the MITgcm tends to have weaker currents, both because it is lower resolution than POP and because the state estimation penalizes structure that does not match the observations or that is not observed. POP is more energetically consistent as it is not constrained to match observations, and may be better at simulating eddies, which are notably present in the CTD/float climatology.

The circulation pattern differs between observations and model results most noticeably near the coast, where large variability exists (see Figure 4c,d). The MITgcm (Figure 6a) shows a striking equatorward flow along the coast, starting at the northwest boundary and extending along the coast of the Philippines; this may be an expression of the Luzon Undercurrent (LUC), which transports intermediate waters equatorward (Qu et al., 1997; Wang et al., 2015). Near 10°N, this current divides into a southward component feeding the MC and an eastward component eddying in the Philippine Sea and feeding the NEUCs. In contrast, POP (Figure 6b) and the CTD/float climatology (Figure 3f) show weak poleward currents near the coast at depths below 600 m. Glider observations indicate that the equatorward flow of the MC extends to at least 1,000 m near the coast, in agreement with the MITgcm. The differences in near-coast flow among the models and observations underline the fact that this is an area of active research.

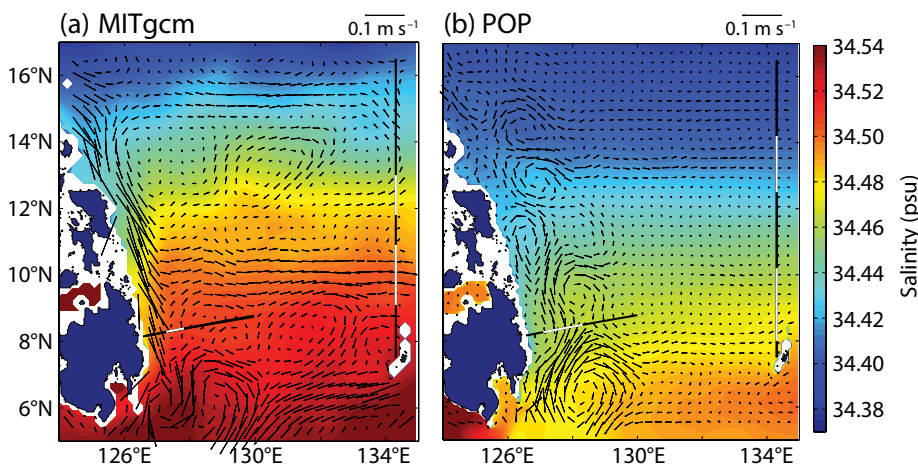


FIGURE 6. Horizontal maps of salinity (color) and velocity (arrows) averaged over the potential density range of 27 to 27.3 kg m⁻³ for (a) the MIT General Circulation Model (MITgcm), and (b) the Parallel Ocean Program (POP) simulation. Black lines show the locations of the objectively mapped mean glider lines across the North Equatorial Current (NEC) and Mindanao Current (MC) during the Origins of the Kuroshio and Mindanao Current project (OKMC) project. Locations for the Mindanao Undercurrent (MUC) and two North Equatorial Undercurrents (NEUCs) for each respective model are shown in white.

Subthermocline Water Mass Transport

Model simulations (Figure 6a,b) and the CTD/float climatology (Figure 3f) suggest that the MUC advects water northward and then eastward, both recirculating and feeding the southern NEUC.

The formation mechanism of the MUC and its connection to the interior ocean subthermocline jets as observed by the CTD/float climatology is explored in Qiu et al. (2015, in this issue). The existence of the LUC near the coast and its connectivity to the MC and the NEUCs is an open question given these observations and models. Glider observations across the MC and NEC provide the water mass transport of the undercurrents that may help to evaluate the modeled circulation.

T-S binned transport diagrams summarize the mean subthermocline transport of the NEUCs (Figure 7a) and the MUC (Figure 7b) by temperature and salinity. These diagrams, constructed using the same binning and averaging as Figure 2b, show the respective undercurrents as positive transport (red). The two NEUCs (Figure 7a), which are located at 9.6°N and 13.1°N in glider observations (Schönau and Rudnick, 2015), each have transports of roughly 5 Sv (Qiu et al., 2015, in this issue). The southern NEUC transports water of a salinity characteristic of AAIW (~34.5 psu), which is slightly greater than that of the northern NEUC (Figure 7a). The MUC (Figure 7b) encompasses the salinity range of the southern NEUC and also a transport of roughly 5 Sv. The mean salinity of the southern NEUC is less than that of the MUC (Figure 7a,b), indicative of mixing between 127°E and 134°E. However, the decrease in salinity may not be accounted for by mixing alone, and may give credence to the explanation that only part of the ~5 Sv of the MUC feeds the southern NEUC, and part of the MUC recirculates south of 8°N. The additional transport of the southern NEUC would then need to come from recirculation of NPIW from the north or by the LUC as suggested by the MITgcm (Figure 6a). The northern NEUC (Figure 7a) and the subthermocline MC (Figure 7b) transport water with salinities between 34.3 and 34.4 psu, of strikingly similar temperatures that are characteristic of interleaved NPIW, supporting the MITgcm representation that these are fed by the LUC.

CONCLUSIONS AND DISCUSSION

Glider and CTD/float observations, complemented by numerical results from two eddy-active ocean general circulation models, have resolved the MC and MUC mean velocity structure, the thermocline and subthermocline transport, and the regional connectivity. The data and model simulations spanned various periods from 2000 to 2014. The observations and results resolve the MC as a strong, surface-intensified, equatorward flow that extends to a depth of 1,000 m near the coast and offshore to 300 km. Centered offshore and deeper than the MC core is a persistent poleward-flowing MUC, with large variability in strength and location. The connectivity of the MC and the MUC to the regional circulation is of interest due to the transport and mixing of water masses of both North and South Pacific origin. The large variability of the subthermocline circulation on interseasonal to decadal time scales makes this an area of active research.

In the representation of the MC and MUC, the glider observations are believed to best capture the mean current structure. Model simulations and CTD/float climatology may not adequately

resolve the flow near the coast. The CTD/float climatology provides geostrophic velocity referenced to a level of no motion at 2,000 m. This reference may be appropriate away from the boundary but not in the swift western boundary current. As a result, the MC core velocity and transport from the CTD/float climatology are roughly half that of the glider and model simulations. Similarly, the glider observations show the MUC to be slightly offshore, likely the most accurate positioning as it is based on absolute velocity observations. The subthermocline variability of the model simulations exceeds the strength of the mean structure, leading to the conclusion that the MUC's position and strength are widely variable.

Observations and model simulations agree that the MUC transports some water masses to the southern NEUC, providing a pathway for AAIW. Offshore, there is also evidence that part of the MUC circulates a portion of its transport volume to the south of the NEUC, which recirculates to form an eddy. The most glaring difference between our results from observations and from simulations is the direction and magnitude of subthermocline velocity near the coast.

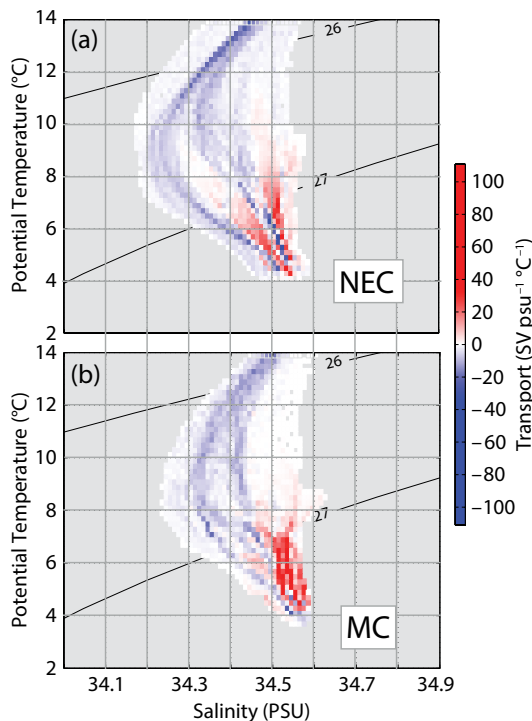


FIGURE 7. An enlarged view of the temperature-salinity (T-S) properties of the subthermocline transport from the glider section across (a) the North Equatorial Current (NEC), and (b) the Mindanao Current (MC). The transport is binned and averaged following Figure 2b. Negative (blue) indicates westward transport of the NEC in panel (a) and equatorward transport of the MC in panel (b). Positive (red) indicates eastward transport of the two North Equatorial Undercurrents (NEUCs) in panel (a) and poleward transport of the MUC in panel (b).

This difference may be related to variability of the MUC, the resolution near the coast, and the reference velocity used in the observations. Near the coast, glider observations and the MITgcm show net equatorward flow, and the CTD/float climatology and POP show net poleward flow. The glider-observed equatorward transport of interleaved NPIW supports the dynamical representation by MITgcm, making it plausible that the NPIW is coming from a northern source such as the LUC. However, the differences between observations and model simulations suggest that more study of variability in this region is needed. 

REFERENCES

- Bell, J.D. 2013. Mixed responses of tropical Pacific fisheries and aquaculture to climate change. *Nature Climate Change* 3(6):591–599, <http://dx.doi.org/10.1038/nclimate1838>.
- Bingham, F.M., and R. Lukas 1994. The southward intrusion of North Pacific Intermediate Water along the Mindanao coast. *Journal of Physical Oceanography* 24(1):141–154, [http://dx.doi.org/10.1175/1520-0485\(1994\)024<0141:TSIONP>2.0.CO;2](http://dx.doi.org/10.1175/1520-0485(1994)024<0141:TSIONP>2.0.CO;2).
- Bingham, F.M., and R. Lukas 1995. The distribution of intermediate water in the western equatorial Pacific during January–February 1986. *Deep Sea Research Part I* 42(9):1,545–1,573, [http://dx.doi.org/10.1016/0967-0637\(95\)00064-D](http://dx.doi.org/10.1016/0967-0637(95)00064-D).
- Davis, R.E., W.S. Kessler, and J.T. Sherman. 2012. Gliders measure western boundary current transport from the South Pacific to the equator. *Journal of Physical Oceanography* 42(11):2,001–2,013, <http://dx.doi.org/10.1175/JPO-D-12-022.1>.
- Dukowicz, J.K., and R.D. Smith 1994. Implicit free-surface method for the Bryan-Cox-Semtner ocean model. *Journal of Geophysical Research* 99(C4):7,991–8,014, <http://dx.doi.org/10.1029/93JC03455>.
- Ffield, A., and A.L. Gordon. 1992. Vertical mixing in the Indonesian thermocline. *Journal of Physical Oceanography* 22:184–195, [http://dx.doi.org/10.1175/1520-0485\(1992\)022<0184:VMITIT>2.0.CO;2](http://dx.doi.org/10.1175/1520-0485(1992)022<0184:VMITIT>2.0.CO;2).
- Fine, R.A., R. Lukas, F.M. Bingham, M.J. Warner, and R.H. Gammon. 1994. The western equatorial Pacific: A water mass crossroads. *Journal of Geophysical Research* 99(C12):25,063–25,080, <http://dx.doi.org/10.1029/94JC02277>.
- Ganachaud, A., S. Cravatte, A. Melet, A. Schiller, N.J. Holbrook, B.M. Sloyan, M.J. Widlansky, M. Bowen, J. Verron, P. Wiles, and others. 2014. The Southwest Pacific Ocean circulation and climate experiment (SPICE). *Journal of Geophysical Research* 119(11):7,660–7,686, <http://dx.doi.org/10.1002/2013JC009678>.
- Gordon, A.L. 1986. Interocean exchange of thermocline water. *Journal of Geophysical Research* 91(C4):5,037–5,046, <http://dx.doi.org/10.1029/JC091iC04p05037>.
- Gouretski, V.V., and K.P. Koltermann. 2004. *WOCE Global Hydrographic Climatology: A Technical Report*, vol. 35. Bundesamt für Seeschifffahrt und Hydrographie, Hamburg, Germany, 52 pp.
- Gu, D., and S.G. Philander. 1997. Interdecadal climate fluctuations that depend on exchanges between the tropics and extratropics. *Science* 275:805–807, <http://dx.doi.org/10.1126/science.275.5301.805>.
- Heimbach, P., C. Hill, and R. Giering. 2002. Automatic generation of efficient adjoint code for a parallel Navier-Stokes solver. *Computational Science—CCS 2002*, International Conference Amsterdam, The Netherlands, April 21–24, 2002, http://dx.doi.org/10.1007/3-540-46080-2_107.
- Hu, D., W. Cai, A. Ganachaud, W.S. Kessler, and J. Sprintall. 2015a. Introduction to special section on Western Pacific Ocean Circulation and Climate. *Journal of Geophysical Research* 120(5):3,175–3,176, <http://dx.doi.org/10.1002/2015JC010856>.
- Hu, D., L. Wu, W. Cai, A.S. Gupta, A. Ganachaud, B. Qiu, A.L. Gordon, X. Lin, Z. Chen, S. Hu, and others. 2015b. Pacific western boundary currents and their roles in climate. *Nature* 522:299–308, <http://dx.doi.org/10.1038/nature14504>.
- Hu, D.X., M.C. Cui, T.D. Ou, and Y.X. Li. 1991. A subsurface northward current off Mindanao identified by dynamic calculation. *Oceanography of Asian Marginal Seas* 54:359–365, [http://dx.doi.org/10.1016/S0422-9894\(08\)70108-9](http://dx.doi.org/10.1016/S0422-9894(08)70108-9).
- Kashino, Y. 2005. Variability of the Mindanao Current: Mooring observation results. *Geophysical Research Letters* 32, L18611, <http://dx.doi.org/10.1029/2005GL023880>.
- Kashino, Y., A. Atmadipoera, Y. Kuroda, and Lukijanto. 2013. Observed features of the Halmahera and Mindanao eddies. *Journal of Geophysical Research* 118(12):6,543–6,560, <http://dx.doi.org/10.1002/2013JC009207>.
- Kashino, Y., I. Ueki, and H. Sasaki. 2015. Ocean variability east of Mindanao: Mooring observations at 7°N, revisited. *Journal of Geophysical Research* 120:2,540–2,554, <http://dx.doi.org/10.1002/2015JC010703>.
- Large, W.G., and S.G. Yeager. 2009. The global climatology of an interannually varying air–sea flux data set. *Climate Dynamics* 33:341–364, <http://dx.doi.org/10.1007/s00382-008-0441-3>.
- Le Dimet, F.-X., and O. Talagrand. 1986. Variational algorithms for analysis and assimilation of meteorological observations: Theoretical aspects. *Tellus A* 38A(2):97–110, <http://dx.doi.org/10.1111/j.1600-0870.1986.tb00459.x>.
- Lindstrom, E., R. Lukas, R. Fine, E. Firing, S. Godfrey, G. Meyers, and M. Tsuchiya. 1987. The western equatorial Pacific Ocean circulation study. *Nature* 330:533–537, <http://dx.doi.org/10.1038/330533a0>.
- Lukas, R., E. Firing, P. Hacker, P.L. Richardson, C.A. Collins, R. Fine, and R. Gammon. 1991. Observations of the Mindanao Current during the western equatorial Pacific Ocean circulation study. *Journal of Geophysical Research* 96(C4):7,089–7,104, <http://dx.doi.org/10.1029/91JC00062>.
- Lukas, R., T. Yamagata, and J.P. McCreary. 1996. Pacific low-latitude western boundary currents and the Indonesian throughflow. *Journal of Geophysical Research* 101(C5):12,209–12,216, <http://dx.doi.org/10.1029/96JC01204>.
- Marshall, J., A. Adcroft, L. Perelman, and C. Heisey. 1997. A finite-volume, incompressible Navier Stokes model for studies of the ocean on parallel computers. *Journal of Geophysical Research* 102:5,753–5,766, <http://dx.doi.org/10.1029/96JC02775>.
- Qiu, B., S. Chen, and H. Sasaki. 2013a. Generation of the North Equatorial Undercurrent jets by triad baroclinic Rossby wave interactions. *Journal of Physical Oceanography* 43(12):2,682–2,698, <http://dx.doi.org/10.1175/JPO-D-13-099.1>.
- Qiu, B., and R. Lukas. 1996. Seasonal and interannual variability of the North Equatorial Current, the Mindanao Current, and the Kuroshio along the Pacific western boundary. *Journal of Geophysical Research* 101(C5):12,315–12,330, <http://dx.doi.org/10.1029/95JC03204>.
- Qiu, B., D.L. Rudnick, I. Cerovecki, B.D. Cornuelle, S. Chen, M.C. Schönau, J.L. McClean, and G. Gopalakrishnan. 2015. The Pacific North Equatorial Current: New insights from the origins of the Kuroshio and Mindanao Currents (OKMC) Project. *Oceanography* 28(4):24–33, <http://dx.doi.org/10.5670/oceanog.2015.78>.
- Qiu, B., D.L. Rudnick, S. Chen, and Y. Kashino. 2013b. Quasi-stationary North Equatorial Undercurrent jets across the tropical North Pacific Ocean. *Geophysical Research Letters* 40:2,183–2,187, <http://dx.doi.org/10.1002/grl.50394>.
- Qu, T., T.-L. Chiang, C.-R. Wu, P. Dutrieux, and D. Hu. 2012. Mindanao Current/Undercurrent in an eddy-resolving GCM. *Journal of Geophysical Research* 117, C06026, <http://dx.doi.org/10.1029/2011JC007838>.
- Qu, T., T. Kagimoto, and T. Yamagata. 1997. A subsurface countercurrent along the east coast of Luzon. *Deep Sea Research Part I* 44(3):413–423, [http://dx.doi.org/10.1016/S0967-0637\(96\)00121-5](http://dx.doi.org/10.1016/S0967-0637(96)00121-5).
- Qu, T., and R. Lukas. 2003. The bifurcation of the North Equatorial Current in the Pacific. *Journal of Physical Oceanography* 33(1):5–18, [http://dx.doi.org/10.1175/1520-0485\(2003\)033<0005:TBOTNE>2.0.CO;2](http://dx.doi.org/10.1175/1520-0485(2003)033<0005:TBOTNE>2.0.CO;2).
- Qu, T., and E.J. Lindstrom. 2004. Northward intrusion of Antarctic Intermediate Water in the western Pacific. *Journal of Physical Oceanography* 34(9):2,104–2,118, [http://dx.doi.org/10.1175/1520-0485\(2004\)034<2104:NIOAIW>2.0.CO;2](http://dx.doi.org/10.1175/1520-0485(2004)034<2104:NIOAIW>2.0.CO;2).
- Qu, T., H. Mitsudera, and T. Yamagata. 1998. On the western boundary current in the Philippine Sea. *Journal of Geophysical Research* 103:7,537–7,548, <http://dx.doi.org/10.1029/98JC00263>.
- Rudnick, D.L., S. Jan, and C.M. Lee. 2015. A new look at circulation in the western North Pacific. *Oceanography* 28(4):16–23, <http://dx.doi.org/10.5670/oceanog.2015.77>.
- Schönau, M.C., and D.L. Rudnick. 2015. Glider observations of the North Equatorial Current in the western tropical Pacific. *Journal of Geophysical Research* 120:3,586–3,605, <http://dx.doi.org/10.1002/2014JC010595>.
- Sherman, J., R.E. Davis, W.B. Owens, and J. Valdes. 2001. The autonomous underwater glider “Spray.” *IEEE Journal of Oceanic Engineering* 26(4):437–446, <http://dx.doi.org/10.1109/48.972076>.
- Smith, W.H.F., and D.T. Sandwell. 1997. Global sea-floor topography from satellite altimetry and ship depth soundings. *Science* 277:1,957–1,962, <http://dx.doi.org/10.1126/science.277.5334.1956>.
- Todd, R.E., D.L. Rudnick, M.R. Mazloff, R.E. Davis, and B.D. Cornuelle. 2011. Poleward flows in the southern California Current System: Glider observations and numerical simulation. *Journal of Geophysical Research* 116, C02026, <http://dx.doi.org/10.1029/2010JC006536>.
- Toole, J.M., R.C. Millard, Z. Wang, and S. Pu. 1990. Observations of the Pacific North Equatorial Current bifurcation at the Philippine coast. *Journal of Physical Oceanography* 20(2):307–318, [http://dx.doi.org/10.1175/1520-0485\(1990\)020<0307:OOPNE>2.0.CO;2](http://dx.doi.org/10.1175/1520-0485(1990)020<0307:OOPNE>2.0.CO;2).
- Tsuchiya, M. 1991. Flow path of the Antarctic Intermediate Water in the western equatorial South Pacific Ocean. *Deep Sea Research Part A* 38(Supplement 1):S273–S279, [http://dx.doi.org/10.1016/S0198-0149\(12\)80013-6](http://dx.doi.org/10.1016/S0198-0149(12)80013-6).

- Tsuchiya, M., R. Lukas, R.A. Fine, E. Firing, and E. Lindstrom. 1989. Source waters of the Pacific equatorial undercurrent. *Progress in Oceanography* 23(2):101–147, [http://dx.doi.org/10.1016/0079-6611\(89\)90012-8](http://dx.doi.org/10.1016/0079-6611(89)90012-8).
- Wang, F., N. Zang, Y. Li, and D. Hu. 2015. On the subsurface countercurrents in the Philippine Sea. *Journal of Geophysical Research* 120:131–144, <http://dx.doi.org/10.1002/2013JC009690>.
- Wijffels, S.E., E. Firing, and J. Toole. 1995. The mean structure and variability of the Mindanao Current at 8°N. *Journal of Geophysical Research* 100(C9):18,421–18,435, <http://dx.doi.org/10.1029/95JC01347>.
- Wunsch, C. 1996. *The Ocean Circulation Inverse Problem*. Cambridge University Press, Cambridge, UK, 458 pp., <http://dx.doi.org/10.1017/CBO9780511629570>.
- Wyrtki, K. 1961. Scientific results of marine investigations of the South China Sea and the Gulf of Thailand 1959–1961. *NAGA Report*, vol. 2. Scripps Institution of Oceanography, La Jolla, CA, <http://escholarship.org/uc/item/49n9x3t4>.
- Yang, Y.J., S. Jan, M.-H. Chang, J. Wang, V. Mensah, T.-H. Kuo, C.-J. Tsai, C.-Y. Lee, M. Andres, L.R. Centurioni, and others. 2015. Mean structure and fluctuations of the Kuroshio East of Taiwan from in situ and remote observations. *Oceanography* 28(4):74–83, <http://dx.doi.org/10.5670/oceanog.2015.83>.
- Zhang, L., D. Hu, S. Hu, F. Wang, F. Wang, and D. Yuan. 2014. Mindanao Current/Undercurrent measured by a subsurface mooring. *Journal of Geophysical Research* 119(6):3,617–3,628, <http://dx.doi.org/10.1002/2013JC009693>.
- Zhang, Y., W.B. Rossow, A.A. Lacis, V. Oinas, and M.I. Mishchenko. 2004. Calculation of radiative fluxes from the surface to top of atmosphere based on ISCCP and other global data sets: Refinements of the radiative transfer model and the input data. *Journal of Geophysical Research* 109, D19105, <http://dx.doi.org/10.1029/2003JD004457>.

ACKNOWLEDGMENTS

This study was supported by the Office of Naval Research (ONR) project Origins of the Kuroshio and Mindanao Currents (OKMC): N00014-10-1-0273 (DLR, JLM, BDC, MCS, IC and GG), N00013-11-1-0429 (DLR and MCS), and N00014-10-1-0267 (BQ). The global CESM simulation was conducted using computer resources (Yellowstone) (<ark:/85065/d7wd3xhc>) provided by the Climate Simulation Laboratory at the National Center for Atmospheric Research (NCAR) Computational and Information Systems Laboratory. JLM and IC were also supported by a US Department of Energy (DOE) Office of Science grant, “Ultra-High Resolution Global Climate Simulation,” via a Los Alamos National Laboratory subcontract. We thank Lori and Pat Colin at the Coral Reef Research Foundation in Palau for glider deployment support, and the Instrument Development Group at Scripps Institution of Oceanography for all operations of the Spray gliders, including Jeff Sherman, Kyle Grindley, Brent Jones, Evan Randall-Goodwin, and Derek Vana. We thank an anonymous reviewer for critical feedback and recommendations for this paper. Argo data were collected and made freely available by the international Argo Program and the national programs that contribute to it (<http://www.argo.ucsd.edu>, <http://argo.jcommops.org>). The Argo Program is part of the Global Ocean Observing System.

AUTHORS

Martha C. Schönau (mcschonau@ucsd.edu) is a graduate student, **Daniel L. Rudnick** is a professor, **Ivana Cerovecki** and **Ganesh Gopalakrishnan** are project scientists, and **Bruce D. Cornuelle** and

Julie L. McClean are research oceanographers at Scripps Institution of Oceanography, University of California, San Diego, La Jolla, CA, USA. **Bo Qiu** is Professor, Department of Oceanography, University of Hawaii at Manoa, Honolulu, HI, USA.

ARTICLE CITATION

Schönau, M.C., D.L. Rudnick, I. Cerovecki, G. Gopalakrishnan, B.D. Cornuelle, J.L. McClean, and B. Qiu. 2015. The Mindanao Current: Mean structure and connectivity. *Oceanography* 28(4):34–45, <http://dx.doi.org/10.5670/oceanog.2015.79>.